

## Simulation of Thin Film Delamination Under Thermal Loading

L. Chernin<sup>1</sup> and K.Y. Volokh<sup>1,2</sup>

**Abstract:** The conventional approach to analysis of thin film delamination is based on the consideration of the film, which is subjected to residual stresses arising from the thermal mismatch between the film and the substrate, within the framework of the classical fracture mechanics and the structural buckling theories. Such concepts as the energy release rate and the stress intensity factors are crucial in this case.

A different approach to analysis of thin film delamination considers the effect of the compliant interface between the film and the substrate. This compliant interface is described by the traction-separation constitutive law.

In the present work, a framework for modeling delamination of thin films is described in accordance with the latter 'decohesion' approach. The film is modeled as a geometrically nonlinear elastic beam attached to a rigid substrate with a cohesive layer of zero thickness. The cohesive layer is described by normal and tangential tractions and corresponding displacement jumps. An exponential 'softening' constitutive law relates tractions and displacements of the cohesive layer. Such formulation allows for studying nucleation, propagation and arrest of local delaminations – edge cracks and blisters. This is in contrast to the traditional approach of the classical fracture mechanics where stress analysis is separated from a description of the actual process of material failure.

Finite element analyses are carried out for the qualitative study of the influence of different parameters of the thin film and the cohesive layer as well as different thermal loads on delamination behavior of the film-substrate system. The results of the analysis show that the stability of the delamination propagation depends mainly on the shape of the thermal load and less on the distribution of the cohesive surface strength along the film. The location of the nucleation of the film separation is essentially sensitive to the combination of the cohesion properties

of the film/substrate interface and the thermal load shape and fewer to the film geometrical defects. It is found that the interior blisters – the arrested delamination processes – are created only for special cases of the film and cohesion property combinations, otherwise the unstable interior delaminations or edge cracks take place. The material imperfection of the film – the inhomogeneous thermal expansion coefficient distribution along the film increases or decreases the effect of the thermal load on the film response and has a little effect on the film delamination process.

### 1 Introduction

Thin films occur in a wide variety of applications – wear-resistant coatings in metal-cutting tools, polymer coatings in optical devices, ceramic thermal barrier coatings in the high-temperature machinery – to list a few. They are used in electronic, aircraft, optic, and automobile industries. Delamination, i.e. debonding between the film and substrate is a typical failure mode of the coatings. In this case local internal *blisters* (also called *buckles* or *wrinkles*) and edge cracks nucleate and propagate. This has a detrimental effect on the coated device and, in the case of thermal coating, can initiate an abrupt damage of the machinery.

The interest in the delamination phenomenon has been growing in the last quarter of the twentieth century; many scientists have investigated this phenomenon in different areas, and many researches were done (Hutchinson and Suo, 1992; Hutchinson, 2001). It began, probably, with the work of Kachanov (1976, 1988), who computed the critical load for the growth of a thin circular delamination in an axisymmetrically compressed plate on the basis of the linear post-buckling equations. Shield et al. (1992, 1994) investigated the buckling of a stiff elastic layer bonded to an elastic half-space under a transverse compressive plane strain. Sheinman et al. (1998) studied a single delamination on a one-dimensional model of a composite laminate structure including the delami-

<sup>1</sup> Faculty of Civil and Environmental Engineering, Technion, Haifa 32000, Israel.

<sup>2</sup> corresponding author: cvolokh@tx.technion.ac.il

nation growth during pre- or post-buckling phases with a wide range of parameters, like imperfection, location of delamination, length-to-thickness ratio etc. More recently, Frostig and Sokolinsky (2000) analyzed the effect of a pre-existing crack on the buckling behavior of sandwich panels with transversely flexible cores. The effect of a finite interfacial compliance on the stability of a thin layer bonded to a substrate was investigated by Bigoni et al. (1997). The dynamic 2D simulations of delamination failure of thin composite plates subjected to low-velocity impact are given by Geubelle and Baylor (1998). Alfano and Crisfield (2001) gave the finite element approach to the delamination analysis of laminated composites using interface elements and interface damage law. In parallel with the general work on delamination a more specific research on the delamination of thin films was performed. Evans and Hutchinson (1984) studied the delamination and spalling of compressed films and coatings using a combination of elastic fracture mechanics and post-buckling theory of plates. More recently, Evans and Hutchinson (1995) overviewed on the different failure modes, like delamination and cracking of brittle layers, thermomechanical fatigue of metallic constituents and interface decohesion, that occur in thin films and multilayers due to residual stress, both thermal and “intrinsic” including stress redistributions and relaxations, plastic dissipation, friction, cyclic load and layer thickness effects. Choi et al. (1999) investigated various delamination types of thermal barrier coatings and thermally growth oxide layers including single layer film delamination, “large” and “small” delaminations of multilayer films. Gioia and Ortiz (1997) studied the buckling-driven delamination mechanism in the compressed thin films leading to forming of blisters that appear when some area of the film buckles away from the substrate.

Most of the works on thin film delamination follow the conventional fracture mechanics approach where stress analysis is separated from a description of the actual process of material failure. The cornerstone of the classical approach to fracture mechanics of Griffith-Orowan-Irwin is a mathematical crack within linear elasticity. The stress field at the tip of the crack is singular and the coefficients of the asymptotic expansions of the stress field near the crack tip – Stress Intensity Factors – are the main players in the Linear Elastic Fracture Mechanics. Generalized fracture considerations allowing for the material nonlinearity in the vicinity of the crack tip are also

based on the SIF concept. Successful application of the classical fracture mechanics to a wide range of engineering materials represents a significant progress beyond the classical strength-of-materials approach which tends to ignore the initiation and growth of crack-like flaws as the ultimate cause of structural failure. However, the established theory of fracture mechanics has serious limitations in several aspects. For example, in thin film devices, plastic flow in metal layers is often severely constrained by the neighboring structure, causing the plastic dissipation part of the overall fracture energy to be a strong function of the device geometry. When this is the case, the fracture toughness – a critical value of SIF – becomes length scale dependent and can no longer be regarded as an intrinsic material property. The nonphysical stress singularity at the crack tip does not appear in a different approach to fracture pioneered by Barenblatt (1959). The idea is to describe fracture as a material separation across a surface. It appears by name of the Cohesive Zone Model in the modern literature. The cohesive zone is a surface in a bulk material where displacement discontinuities occur. Thus, continuum is enhanced with discontinuities. The latter requires an additional constitutive description. Equations relating normal and tangential displacement jumps across the cohesive surfaces with the proper tractions define a specific CZM. There is a plenty of proposals of the ‘cohesive’ constitutive equations, for example, Barenblatt (1959); Dugdale (1960); Needleman (1987); Rice and Wang (1989); Tvergaard and Hutchinson (1992); Xu and Needleman (1994); Camacho and Ortiz (1996); Geubelle and Baylor (1998); Chandra et al. (2002); Foulk et al. (2000); Mohammed and Liechti (2000); Needleman (1987); Rahul Kumar et al. (2000); Stroud et al. (2002); Givoli (2004); Li and Siegmund (2004). All these models are constructed qualitatively as follows: tractions increase, reach a maximum, and then approach zero with increasing separation. This scenario is in harmony with the intuitive understanding of the rupture process. Needleman (1987) introduced the cohesive zone models in computational practice. Since then CZMs are used increasingly in finite element simulations of crack tip plasticity and creep; crazing in polymers; adhesively bonded joints; interface cracks in bimetals; delamination in composites and multilayers; fast crack propagation in polymers and etc. Crack nucleation, propagation, branching, kinking, and arrest are a natural outcome of the computations where the discontinuity surfaces are spread over the bulk material.

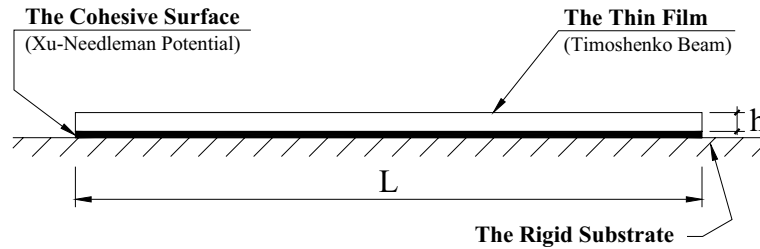


**Figure 1 :** The model of a thin film attached to a rigid substrate.

In this work a one-dimensional model of a thin film attached to a rigid substrate with a CZM is chosen in order to simulate the qualitative film behavior for various load and condition types. The problem formulation allows for tracing nucleation, propagation and arrest of local delaminations – edge cracks and blisters. The film is considered as a geometrically nonlinear elastic beam where cross-sections remain straight and not perpendicular to the neutral axis after deformation – the nonlinear Timoshenko beam. The CZM is described by normal and tangential tractions and corresponding displacements. An exponential separation constitutive law relating tractions and displacements is introduced. Finite element analysis is carried out for the study of the influence of different parameters of the thin film and the cohesive layer as well as different thermal loads on delamination behavior of the film-substrate system. The results of the analysis show that the stability of the delamination propagation depends mainly on the shape of the thermal load and less on the distribution of the cohesive surface strength along the film. The location of the nucleation of the film separation is essentially sensitive to the combination of the cohesion properties of the film/substrate interface and the thermal load shape and fewer to the film geometrical defects. It is found that the interior blisters – the arrested delamination processes – are created only for special cases of the film and cohesion property combinations, otherwise the unstable interior delaminations or edge cracks take place. The material imperfection of the film – the inhomogeneous thermal expansion coefficient distribution along the film increases or decreases the effect of the thermal load on the film response and has a little effect on the film delamination process.

## 2 Methods

Analytical and computational settings for the mechanics of the film-substrate system are developed in this section.

### 2.1 Problem formulation

The total potential energy of a thin elastic layer attached to a rigid substrate and subject to prescribed tractions and heating may be written in the following form:

$$\Psi = \int_V W dV - \int_{S^*} \phi dS, \quad (1)$$

where  $W$  is the strain energy per unit volume of the layer including thermal strains;  $\phi$  is the potential of the cohesive surface between the layer and the substrate;  $S^*$  is the area of the contact between the layer and the substrate;  $\mathbf{u}$  is a displacement field obtained from the equilibrium equations:

$$\delta\Psi(\mathbf{u}) = 0. \quad (2)$$

Eqs. (1) and (2) represent a particular case of the general formulation for multilayers given by Volokh and Needleman (2002).

We restrict our consideration by one-dimensional problems of a beam-film attached to the substrate. In this case the potential of the cohesive surface can be written as a simplified Xu-Needleman (1994) potential:

$$\phi = \phi_n + \phi_n \left( 1 + \frac{\Delta_n}{\delta_n} \right) \exp \left( -\frac{\Delta_n}{\delta_n} - \frac{\Delta_t^2}{\delta_n^2} \right), \quad (3)$$

where  $\phi_n$  is the work of separation;  $\Delta_n = \mathbf{n} \cdot \Delta$  and  $\Delta_t = \mathbf{t} \cdot \Delta$  with  $\mathbf{n}$  and  $\mathbf{t}$  as the unit normal and tangent, respectively, to the surface at the given point in the reference configuration;  $\Delta$  is the displacement jump across the cohesive surface;  $\phi_n$  is the separation work

$$\phi_n = \sigma_{\max} \delta_n \exp(1), \quad (4)$$

where  $\sigma_{\max}$  designate the normal strength of the cohesive surface, while  $\delta_n$  is the corresponding characteristic lengths.

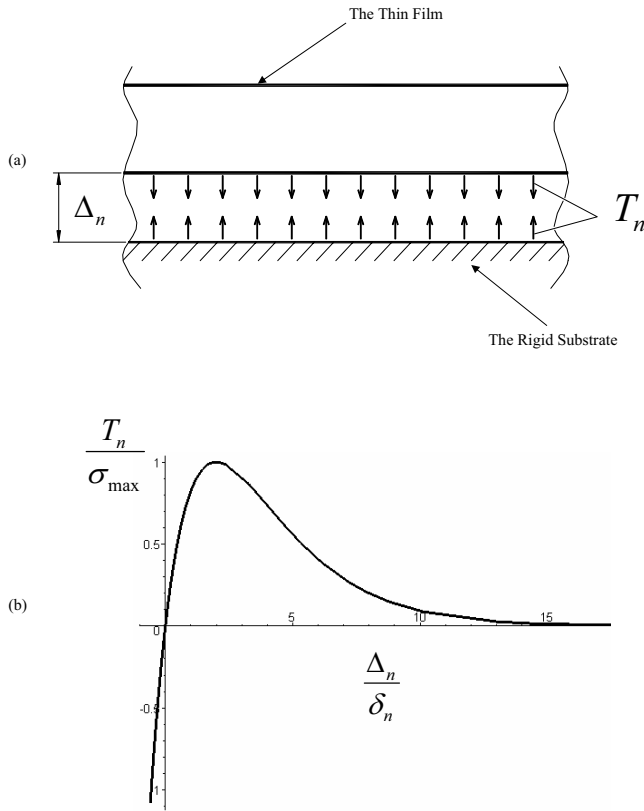


**Figure 2 :** (a) Normal traction,  $T_n$ , and displacements,  $\Delta_n$ ; (b) Traction-separation law for the normal traction,  $T_n$ , as a function of the displacements,  $\Delta_n$ , when  $\Delta_t \equiv 0$ .

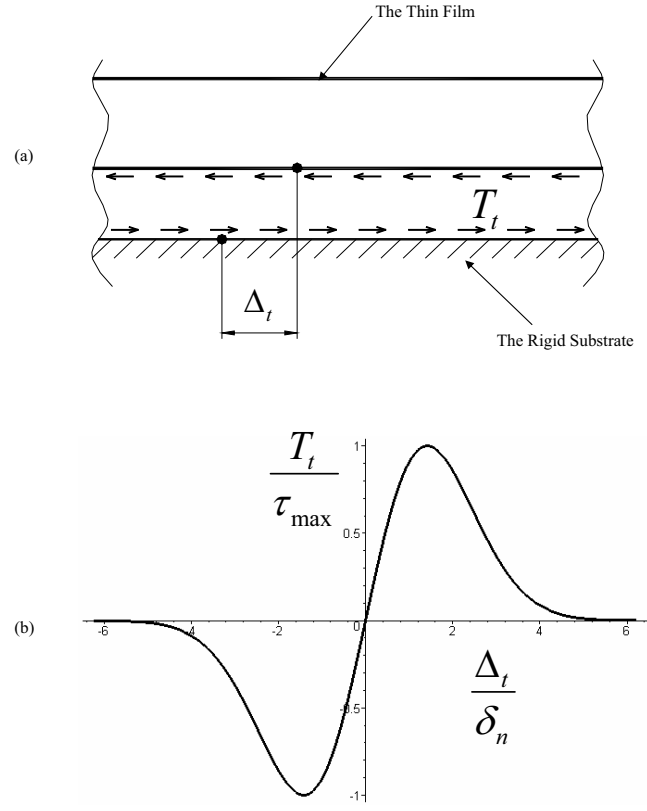


**Figure 3 :** (a) Tangential traction,  $T_t$ , and displacements,  $\Delta_t$ ; (b) Traction-separation law for the tangential traction,  $T_t$ , as a function of the displacements,  $\Delta_t$ , when  $\Delta_n \equiv 0$ .

The cohesive surface tractions are obtained by differentiating potential  $\phi$ :

$$T_n = \frac{\partial \phi}{\partial \Delta_n} = -\frac{\phi_n \Delta_n}{\delta_n^2} \exp\left(-\frac{\Delta_n}{\delta_n} - \frac{\Delta_t^2}{\delta_n^2}\right), \quad (5)$$

$$T_t = \frac{\partial \phi}{\partial \Delta_t} = -2\frac{\phi_n \Delta_t}{\delta_n^2} \left(1 + \frac{\Delta_n}{\delta_n}\right) \exp\left(-\frac{\Delta_n}{\delta_n} - \frac{\Delta_t^2}{\delta_n^2}\right). \quad (6)$$

The variation of  $T_n$  with  $\Delta_n$  when  $\Delta_t \equiv 0$ , and the variation of  $T_t$  with  $\Delta_t$  when  $\Delta_n \equiv 0$  are given in Figures 2 and 3 accordingly. The maximum value of  $T_n$  ( $= \sigma_{\max}$ ) is attained at  $\Delta_n = \delta_n$ , and the maximum value of  $|T_t|$  ( $= \tau_{\max}$ ) is attained at  $|\Delta_t| = \delta_n / \sqrt{2}$ .

Due to the influence of the external loads the thin film can change its geometry and its parts can slide or rise from the substrate. As a result of the geometrical changes the cohesive surface tractions arise at the interface and restrict the separation of the film from the substrate. The tangential traction across the cohesive layer increases

with growing normal displacements (for  $\Delta_n < \delta_n$ ) due to the sliding of the film on the substrate in any direction. After the traction reaches a maximum (when  $\Delta_n = \delta_n$ ), it decreases and falls to zero (for  $\Delta_n > \delta_n$ ) permitting a complete decohesion and simulating the creation of a new free surface. When the film clings and tries to enter the substrate the volume of the normal traction increases very rapidly preventing the entrance. It is obvious, see Eqs. (5) and (6), that both the normal and the shear traction, ( $T_n, T_t$ ), depend non-linearly on the normal as well as on the tangential displacement jump, ( $\Delta_n, \Delta_t$ ), across the cohesive surface. The normal and the shear traction, ( $T_n, T_t$ ), as a functions of the coupling between the normal and the tangential displacement jump, ( $\Delta_n, \Delta_t$ ), across the cohesive surface are presented in Fig.4.

The thin film is considered as a Timoshenko beam, which is appropriate when the half-length of the deformation wave is not less than the film thickness, and the strain

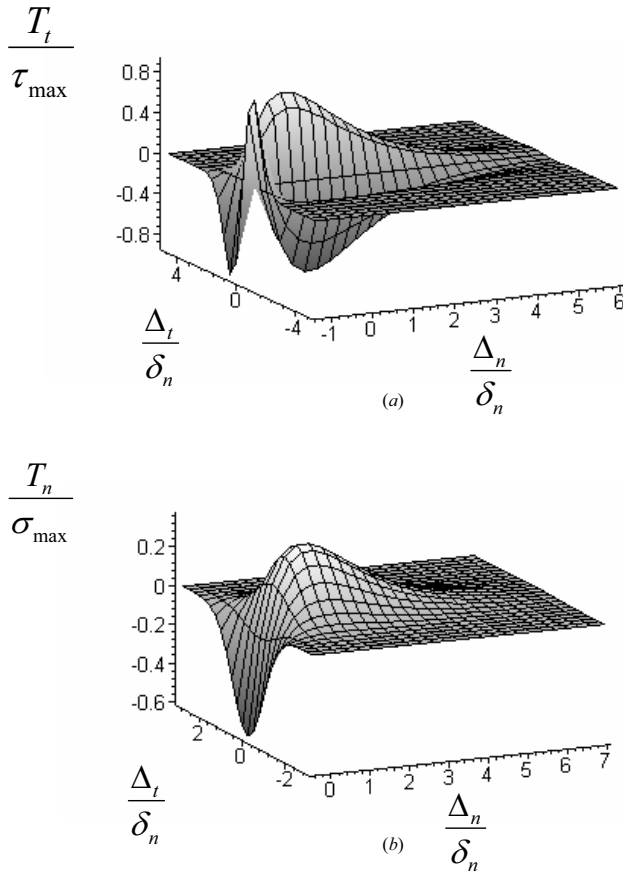


**Figure 4** : Variation of the normal and the shear cohesive tractions,  $(T_n, T_t)$ , with respect to the normal and tangential displacement discontinuities,  $(\Delta_n, \Delta_t)$ : (a) the shear traction,  $T_t$ ; (b) the normal traction,  $T_n$ .

energy takes the form:

$$W = 1/2 \int (EA\varepsilon^2 + EI\chi^2 + GA\gamma^2 - 2EA\alpha T\varepsilon) dx, \quad (7)$$

where  $E$  and  $G$  is the Young and shear modulus, respectively;  $A$  is the cross-sectional area;  $I$  is the moment of inertia;  $\alpha$  is the coefficient of thermal expansion of the film; and  $T$  is the thermal load. For small strains and large rotations the strain measures may be written in the form:

$$\varepsilon = \frac{du}{dx} + \frac{1}{2} \left( \frac{du}{dx} \right)^2 + \frac{1}{2} \left( \frac{dw}{dx} \right)^2, \quad (8)$$

$$\chi = -\frac{d\theta}{dx}, \quad (9)$$

$$\gamma = -\theta + \arcsin \frac{dw}{dx}, \quad (10)$$

where  $u$  is an axial displacement;  $w$  is a transverse displacement; and  $\theta$  is the rotation of the beam cross-section. The non-linear terms in the strain-displacement relations allow excluding large rotations and translations. Thus small strains are superposed on rigid body motions. The latter approach is known as “co-rotational” (Crisfield 1991, 1997). Accounting for geometrical non-linearity is crucial for performing non-linear delamination analysis.

## 2.2 Numerical implementation

The total energy given in Eq. (3.40) is discretized by partitioning the beam-film uniformly into  $n$  elements and index  $i$  designates an element or a node (the left edge of the element) according to assumption that all unknowns,  $(u, w, \theta)$ , are changed linearly within one element

$$\begin{aligned} \Psi(\mathbf{u}, \lambda) = & \frac{L}{m} \sum_{i=1}^m \left( \frac{(EI)_i}{2} \chi_i^2 + \frac{(GA)_i}{2} \gamma_i^2 \right. \\ & \left. + \frac{(EA)_i}{2} \varepsilon_i^2 - \lambda (EA\alpha T)_i \varepsilon_i - b\phi_n \left[ 1 + \frac{\Delta_{ni} + \Delta_{ni+1}}{2\delta_n} \right] \right. \\ & \left. \exp \left\{ -\frac{\Delta_{ni} + \Delta_{ni+1}}{2\delta_n} - \left( \frac{\Delta_{ti} + \Delta_{ti+1}}{2\delta_n} \right)^2 \right\} \right), \quad (11) \end{aligned}$$

where  $(EI)_i$ ,  $(EA)_i$  and  $(GA)_i$  are the bending, axial and shear stiffness of the  $i$ -th element accordingly;  $\lambda$  is a temperature scaling parameter;  $L$  and  $b$  are the film length and width, respectively;  $\varepsilon_i$  and  $\gamma_i$  are the axial and shear strain, respectively, and  $\chi_i$  is the curvature of the  $i$ -th element that take the following form

$$\chi_i = \frac{\theta_i - \theta_{i+1}}{L/m}, \quad (12)$$

$$\varepsilon_i = \frac{u_{i+1} - u_i}{L/m} + \frac{1}{2} \left( \frac{u_{i+1} - u_i}{L/m} \right)^2 + \frac{1}{2} \left( \frac{w_{i+1} - w_i}{L/m} \right)^2, \quad (13)$$

$$\gamma_i = \arcsin \left( \frac{w_{i+1} - w_i}{L/m} \right) - \frac{\theta_{i+1} + \theta_i}{2}, \quad (14)$$

where  $u_i$  and  $w_i$  are an axial and transverse displacement, and  $\theta_i$  is the rotation of the  $i$ -th node.

The normal,  $\Delta_{ni}$ , and tangential,  $\Delta_{ti}$ , displacement jump across the cohesive surface for the  $i$ -th element are

$$\Delta_{ni} = w_i, \quad (15)$$

$$\Delta_{i1} = u_i + \frac{h_i \theta_i}{2}, \quad (16)$$

where  $h_i$  represents the height of the  $i$ -th element.

Cohesive elements, which act like nonlinear springs, are attached to the beam elements and simulate the surface where failure is possible. These nonlinear springs resist opening of the interface crack and sliding of the beam on the substrate in accordance to the prescribed traction-separation relations.

Nonlinear equation solvers allow for tracing the equilibrium path of the beam-film for the prescribed load. In order to follow the equilibrium path in its state space it is useful to introduce the column matrix of 'unbalanced forces', the tangent stiffness matrix, and the column matrix of 'nodal loads' accordingly

$$\mathbf{g} = \frac{\partial \Psi}{\partial \mathbf{u}} = \mathbf{0}, \quad (17)$$

$$\mathbf{K} = \frac{\partial \mathbf{g}}{\partial \mathbf{u}}, \quad (18)$$

$$\mathbf{q} = -\frac{\partial \mathbf{g}}{\partial \lambda}. \quad (19)$$

A variety of approaches exist for solving discrete Eq. (17): Crisfield (1991, 1997); Keller (1992); Riks (1998); Seydel (1994); Kouhia and Mikkola (1989); Magnusson and Svensson (1998).

The basic procedure for tracing a monotonically increasing or decreasing equilibrium path is the Newton-Raphson algorithm:

Box 1:

1. Input: a point on the equilibrium path ( $\mathbf{u}, \lambda, \mathbf{g}, \mathbf{K}, \mathbf{q}$ ).
2. Load increment:  $\lambda \leftarrow \lambda + d\lambda$  and updating  $\mathbf{g}, \mathbf{K}$ .
3. Computation:  $d\mathbf{u} = -\mathbf{K}^{-1}\mathbf{g}$ .
4. Updating:  $\mathbf{u} \leftarrow \mathbf{u} + d\mathbf{u}$  and updating  $\mathbf{g}, \mathbf{K}, \mathbf{q}$ .
5. Go to step 2 if a convergence criterion is satisfied or return to step 3 otherwise.

This algorithm is unable to treat points where the equilibrium path does not exist for increasing parameter  $\lambda$ . Arc-length continuation is better suited to these situations:

Box 2:

1. Input: a point on the equilibrium path ( $\mathbf{u}, \lambda, \mathbf{g}, \mathbf{K}, \mathbf{q}$ ).
2. Arc-length increment:  $ds$ .
3. Predictor (initial guess):  $\mathbf{y} = \mathbf{K}^{-1}\mathbf{q}$ ;  $d\lambda = ds/\sqrt{\mathbf{y}^T\mathbf{y}+1}$ ;  $d\mathbf{u} = \mathbf{y}d\lambda$ .
4. Updating:  $\mathbf{u} \leftarrow \mathbf{u} + d\mathbf{u}$ ;  $\lambda \leftarrow \lambda + d\lambda$  and updating  $\mathbf{g}, \mathbf{K}, \mathbf{q}$ .
5. Corrector:  $\delta\mathbf{v} = \mathbf{K}^{-1}\mathbf{q}$ ;  $\delta\mathbf{w} = \mathbf{K}^{-1}\mathbf{g}$ ;  $\delta\lambda = -(\mathbf{d}\mathbf{u}^T\delta\mathbf{w})/(\mathbf{d}\mathbf{u}^T\delta\mathbf{v})$ ;  $\delta\mathbf{u} = \delta\mathbf{w} + \delta\lambda\delta\mathbf{v}$ .
6. Updating:  $d\mathbf{u} \leftarrow d\mathbf{u} + \delta\mathbf{u}$ ;  $\mathbf{u} \leftarrow \mathbf{u} + \delta\mathbf{u}$ ;  $d\lambda \leftarrow d\lambda + \delta\lambda$ ;  $\lambda \leftarrow \lambda + \delta\lambda$  and updating  $\mathbf{g}, \mathbf{K}, \mathbf{q}$ .
7. Go to step 2 if a convergence criterion is satisfied or return to step 5 otherwise.

It may be seen from Box 2, that the 'arc-length parameter'  $ds$  controls the advance along the equilibrium path and that any turning point is readily treated. In contrast to the Newton-Raphson procedure (Box 1) the first and subsequent iterations are distinguished and called predictor and corrector steps accordingly. Various predictors and correctors have been proposed in the literature: Crisfield (1997); Seydel (1994). It is possible, for example, to find the corrector by applying the Newton-Raphson procedure to some augmented system of nonlinear equations, which include Eq. (2) together with some arc-length constraint. Such an approach is called 'consistent' by some authors (Wriggers, 1995). In this sense, the algorithm given in Box 2 is 'inconsistent'. However, it was found to be efficient in the present computations.

### 3 Results

In this section behavior of a thin metallic film is analyzed under non-uniform thermal loads and non-uniform geometrical and material characteristics of the film.

#### 3.1 General remarks

The geometrical and material properties of the thin elastic layer presenting a metallic film that have been varied in the following range in simulations

$$E = 200 \text{ GPa}, \quad \alpha = 10^{-6} \div 10^{-5} \text{ } 1/^{\circ}\text{C}, \quad \nu = 0.3, \\ h = 0.1 \div 2 \text{ } \mu\text{m}, \quad L = 30 \div 60 \text{ } \mu\text{m}, \quad T = 10^2 \div 10^3 \text{ } ^{\circ}\text{C} \quad (20)$$

where  $E$  is the Young modulus;  $\alpha$  is the coefficient of the thermal expansion;  $\nu$  is the Poisson's ratio;  $L$  and  $h$  are

the length and height of the film;  $T$  is the temperature. The film is assumed to be of the unit width.

The geometrical non-uniformity or the local geometrical defects of the film are modeled by gradual changes in the height of different parts of the film or of its whole length. The material film non-uniformity is simulated by varying the thermal expansion coefficient. The local defects and strength non-uniformity of the cohesive layer are considered by gradual changes in the work of the film-substrate separation.

The cohesive surface properties defining the strength of the bond between the thin film and the substrate are chosen as follows

$$\begin{aligned} \phi_n &= 0 \div 1 \frac{J}{m^2}, \quad \delta_n = 5 \cdot 10^{-4} \mu m, \quad \sigma_{\max} = \frac{\phi_n}{e \delta_n}, \\ \tau_{\max} &= \sqrt{2e} \frac{\phi_n}{e \delta_n}, \quad J_{1C} = \phi_n, \quad K_{1C} = \sqrt{\frac{E J_{1C}}{1 - \nu^2}}, \end{aligned} \quad (21)$$

where  $\phi_n$  is the work of separation per unit crack length required to create the two crack surfaces;  $\delta_n$  is the characteristic length designating the value of the normal and the tangential displacement jump,  $(\Delta_n, \Delta_t)$ , corresponding to the maximal normal and shear traction,  $(T_n = \sigma_{\max}, T_t = \tau_{\max})$ , arising in the interface;  $\sigma_{\max}$  and  $\tau_{\max}$  are the maximal normal and shear stress that the cohesive surface can develop due to the film deformations;  $e$  designates  $\exp(1)$ ;  $J_{1C}$  designates the strain energy release rate during crack growth as calculated for a line crack using the elasticity theory; and  $K_{1C}$  represents the stress intensity factor at the tip of the crack. Here a link to the LEFM is made through the stress intensity factor.

The thin film behavior is analyzed by using the path following techniques considered in the previous section (see Boxes 1, 2). These methods allow for analyzing very complicated problems with high degree of non-linearity. For example, the very sharp limit points and following unload paths arising during the computations are traced successfully (see Figs. 5 and 6).

The delamination of the film from the substrate is assumed as the only failure mode. The interior film or substrate failure is not considered in the present work.

Stable or unstable developments of the film delamination can occur. The unstable delamination means entire decohesion of the film in a dynamic mode because of the instability of the static solution. The stable delamination means creation and gradual development of the edge

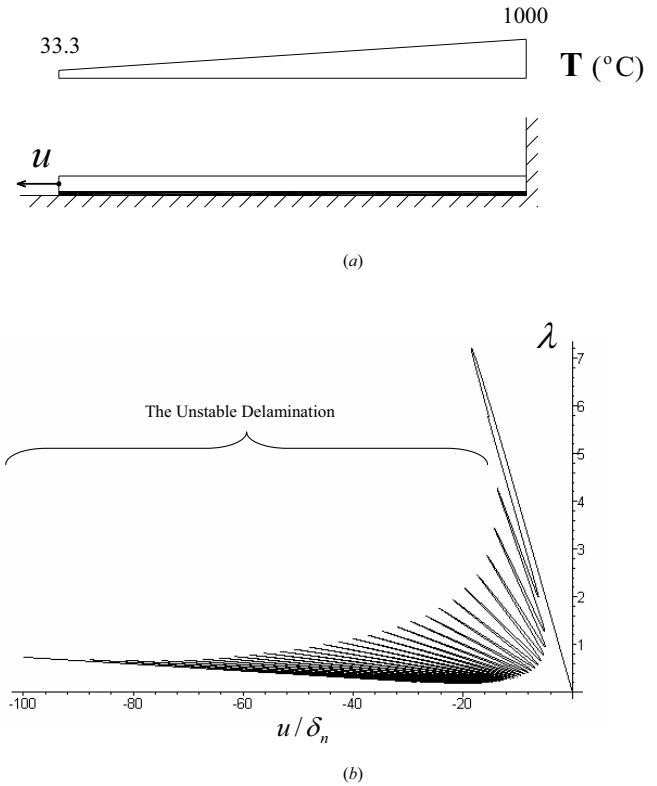


**Figure 5** : A typical case of the unstable delamination. (a) The film under linearly varying thermal load; (b) The horizontal displacement,  $u$ , of the free film edge as a function of the temperature loading parameter  $\lambda$ .

cracks and nucleation of the local interior delaminations – blisters. Two modes of delamination development are possible: (a) the *shearing* delamination arising from the ideal non-frictional sliding of a film along the substrate and (b) the buckling of the film leading to the *opening* of a crack – rising of a film part from a substrate.

The unstable delamination type is shown in Fig. 5. The graph (Fig.5b) presents the horizontal displacement,  $u$ , of the free end of the film, subjected to the conditions shown in Fig.5a, as a function of temperature changes,  $T$ . All sharp peaks appearing on the graph are limit points corresponding to the separation of a single finite element of the film when the normal or the shear traction reaches the maximum value:  $T_n = \sigma_{\max}$  or  $T_t = \tau_{\max}$ . In the presented case the shear delamination type takes place when the crack between the film and the substrate propagates due to the sliding of the film on the substrate and the opening of the crack does not occur (the film clings to the sub-

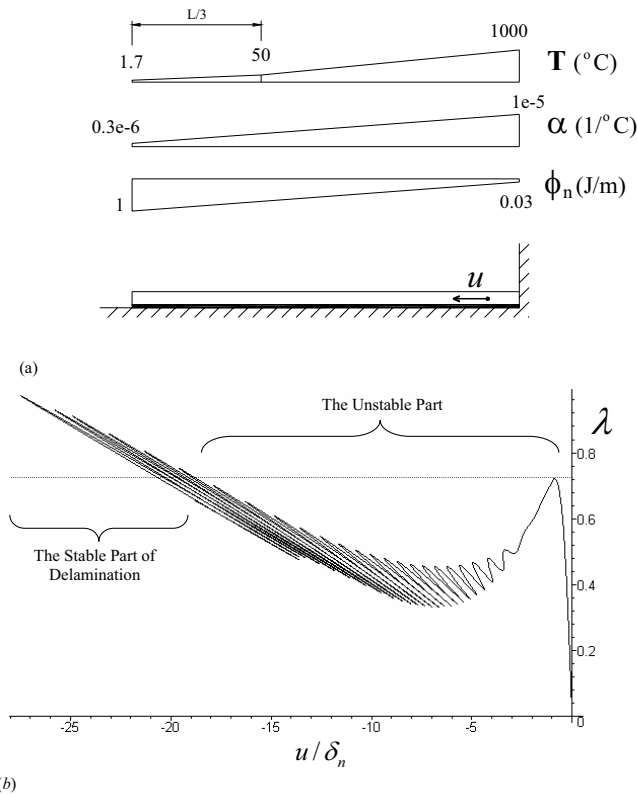


**Figure 6 :** The case of the partial stable delamination (the case of the *blister* creation). (a) The film under presented conditions; (b) The horizontal displacement,  $u$ , of the film near the fixed edge as a function of the temperature loading parameter  $\lambda$ .

strate). It can be seen that the separation value of the thermal load parameter  $\lambda$  of the first finite element ( $\lambda \approx 7$ ) is higher than needed to gain decohesion of the second ( $\lambda \approx 5.5$ ), third ( $\lambda \approx 4$ ), and so on elements. As a result the separation of the film from the substrate is developed dynamically after debonding of the first element.

In Fig.6 the case of partially stable/unstable delamination is presented. It can be seen that the debonding starts unstably and jumps to a stable state. The stable delamination is characterized by the increasing thermal load parameter,  $\lambda$  - Fig.6b. The competing conditions of material and load non-uniformity are presented in Fig.6a. The delamination process starts at the fixed right edge of the film and after unstable propagation is arrested – increasing temperature is needed for the subsequent separation – what means creation of a *blister*. The qualitative behavior of the film under the conditions presented in Figs.

5 and 6 is shown in Figs. 7 and 8 respectively.

The unstable propagation of the delamination in the presented case can lead to the complete decohesion of the beam due to the inertia. The latter requires dynamic analysis, which is beyond the scope of our work.

In simulations considered above and below the film is partitioned in 30 elements of the equal length, if not defined otherwise. The film length is  $L = 30 \mu\text{m}$ ; the film height is  $h = 2 \mu\text{m}$ .

Simulation results are presented for different values of the material parameters in Figs. 7-11. The bold cohesive layer designates perfect bonding. It disappears with debonding. The symbol of the load incremental factor  $\lambda$  is replaced by  $t$  emphasizing the thermal character of the load. The delamination mode for various loading cases is defined by analyzing the values of the load factor  $t$  determined at various stages of debonding.

It is assumed that delamination can propagate in two different modes: (a) due to the sliding of the film on the substrate, called *shearing* or *Mode-II-like*, where the tangent traction of the cohesive surface reaches its maximum value and afterwards decreases to zero; and (b) due to the opening of the crack between the film and the substrate, called *opening* or *Mode-I-like*, occurring when the normal traction increases to its maximum and afterwards decreases to zero.

The boundary conditions of the film for all simulations are chosen free-fixed that permit the creation and the development of both the edge crack (the formation and the spread of the free end delamination) and the *blister* (the nucleation and the propagation of the fixed end delamination).

The cohesive surface strength is regulated in all simulations by the variation of the work separation value  $\phi_n$ . Also the coefficient of the thermal expansion  $\alpha$  and the film thickness are varied.

### 3.2 Simulation cases

The simulation cases for the thin film under thermal loads are presented in Figs. 7-11.

We begin with the comparison of two cases of the non-uniform thermal loading presented in Figs. 7a and 8a. The difference is in the gradient of the thermal load. In the former case the temperature increases from the free edge to the fixed edge. In the latter case the temperature decreases from the left to the right accordingly.



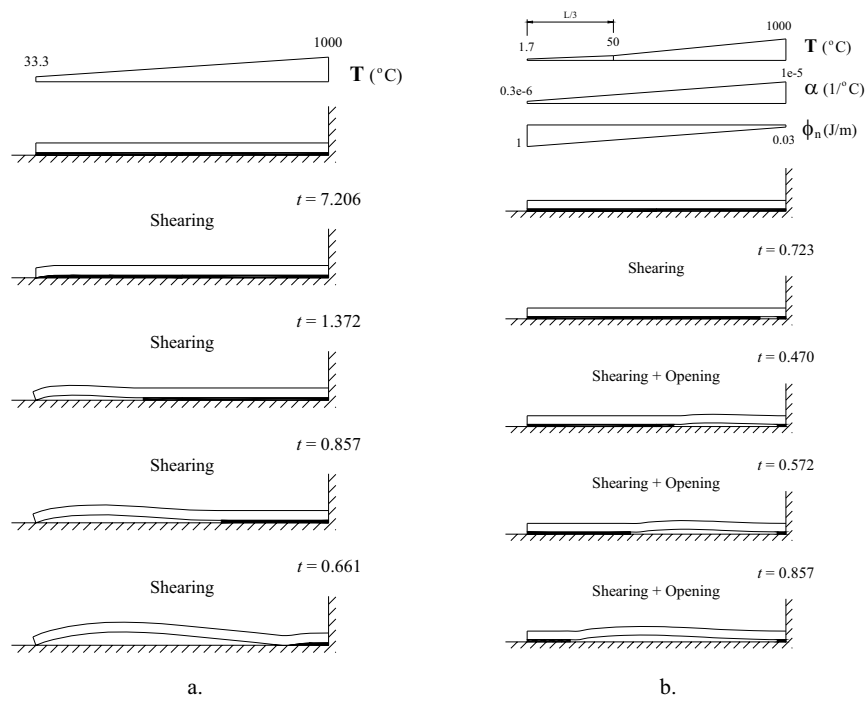


**Figure 7 :** (a) Non-uniform heating of the film – unstable delamination; (b) Non-uniform heating of the film with the non-uniform cohesive surface strength distribution and the film material imperfection – stable delamination with the blister formation.

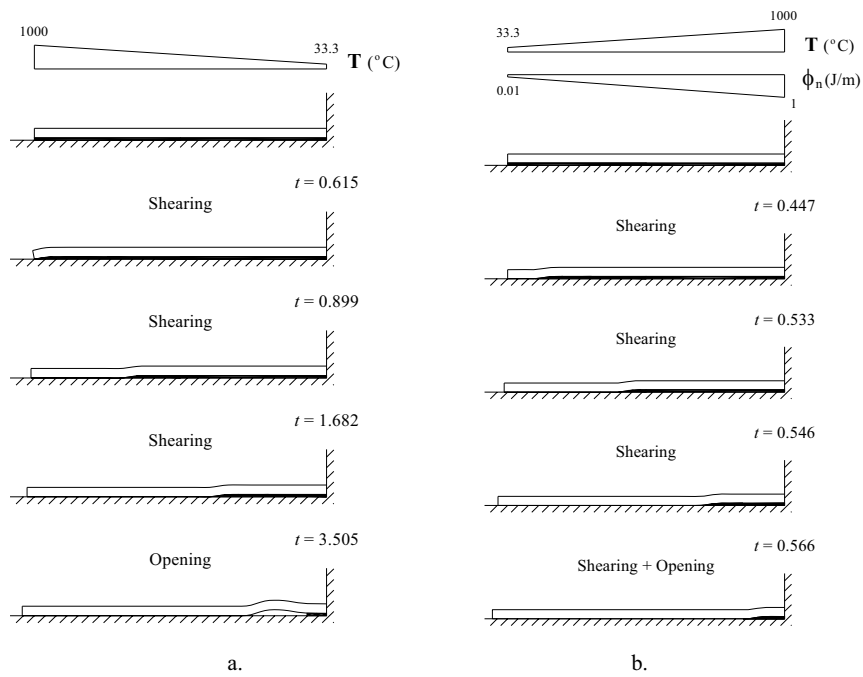


**Figure 8 :** (a) Non-uniform heating of the film – stable delamination; (b) Non-uniform heating of the film with the non-uniform distribution of the cohesive strength – stable delamination.

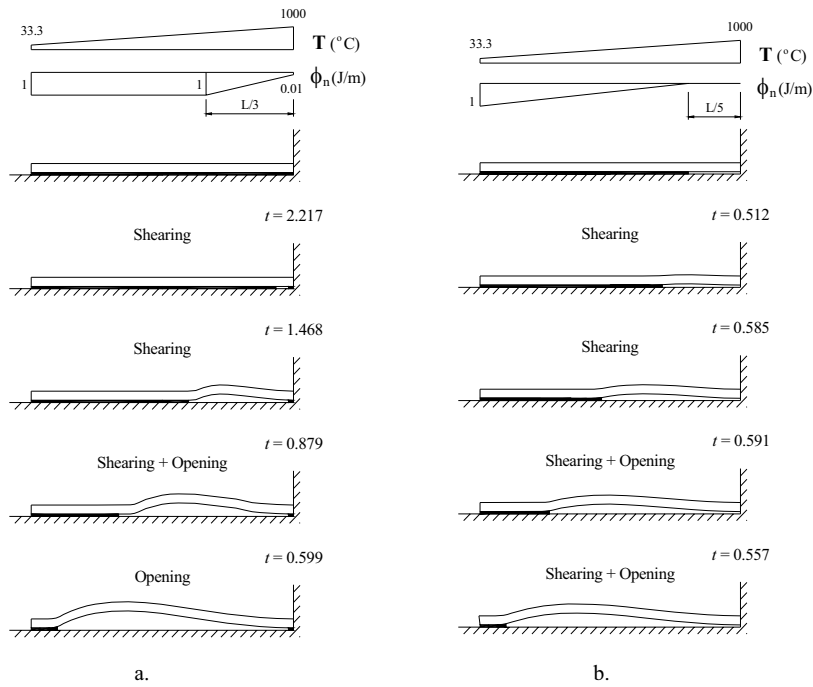


**Figure 9** : (a) Non-uniform heating of the film with the local defect of the cohesive surface – unstable delamination; (b) Non-uniform heating of the film with the initial blister – stable delamination.

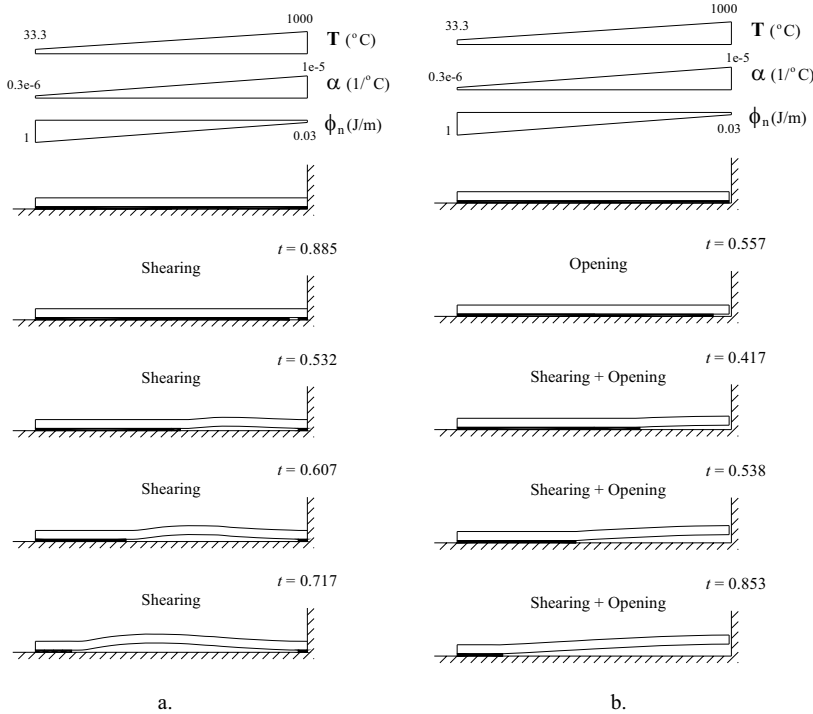


**Figure 10** : (a) Non-uniform heating of the film with the non-uniform distribution of the cohesive strength and the thermal expansion coefficient – unstable delamination (b) Stabilization of the delamination in case (a) by allowing for the vertical displacements at the right edge.

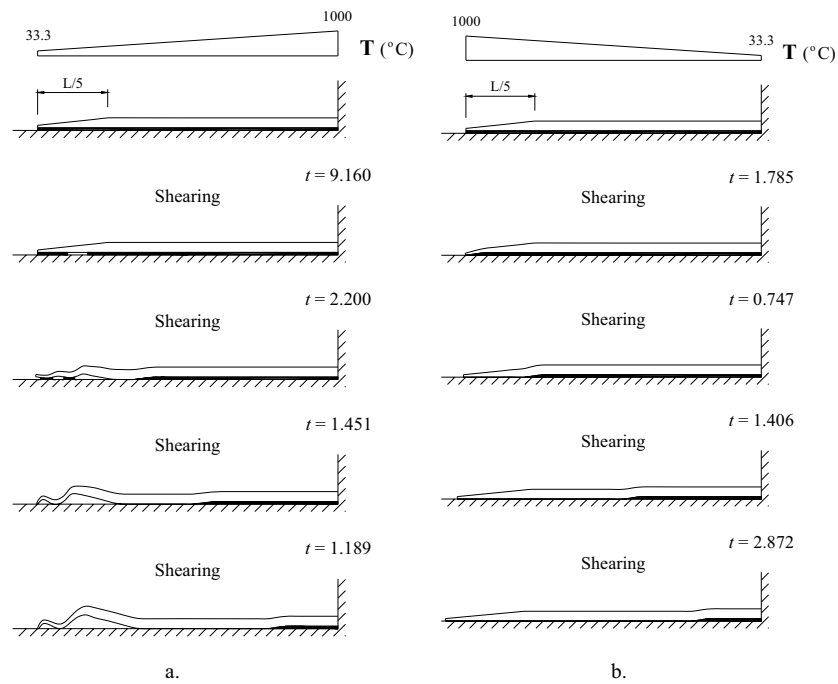


**Figure 11** : (a) Non-uniform heating of the film with the edge thinning – unstable delamination; (b) Non-uniform heating of the film with the edge thinning – stable delamination

In both cases the crack nucleates at the free edge. Its propagation, however, is unstable, i.e. dynamic, in the case shown in Fig.7a, and its propagation is stable, i.e. quasi-static, in the case shown in Fig.8a. The physical reason for such difference is that all film elements in Fig.7a are exposed to the larger thermal loads as compared to the load at the free edge element where debonding starts. Thus delamination propagates in a dynamic mode in Fig.7a. On the contrary, all film elements in Fig.8a are exposed to the lower thermal loads as compared to the load at the free edge element where debonding starts. Thus the rupture of the successive elements requires the increase of the thermal load as shown in Fig.8a.

It is very interesting that the unstable (dynamic) crack propagation for the positive temperature gradient can be 'stabilized' by the non-uniform distribution of the separation parameter (separation work  $\phi_n$ ) along the cohesive layer as shown in Fig.8b. Roughly speaking, the contact between the film and the substrate is weak at the free edge and it is getting stronger towards the fixed edge. In this case the debonding starts at the free edge under the low temperature (as compared to Fig.7a). However, the energy supplied to the crack tip in this case is not enough in

order to separate the successive element and the loading parameter should be increased. The crack grows quasi-statically in a stable mode.

The weak contact between the film and the substrate can essentially affect delamination results. The case where the weak cohesive zone shifts crack nucleation to the right (fixed) edge of the film is shown in Fig.9a. The crack propagates unstably, i.e. dynamically. This case is sensitive to the specific parameters of the contact. A case where the initial crack propagation is stable is shown in Fig.9b. The initial blister at the fixed edge can grow stably up to a certain value of the thermal loading parameter. Then the dynamic delamination takes place.

The case of the weakened contact between the film and the substrate is complicated with the non-uniform distribution of the coefficient of the thermal expansion  $\alpha$  in Fig.10. This leads to the delamination scenario where a blister nucleates inside the film and not at the free edge. Two cases of the unstable and stable blister propagation are given in Fig.10a and Fig.10b, accordingly. The stabilization of the blister in Fig.10b is achieved by allowing for the vertical displacements at the fixed edge – the moving fixed edge.

Finally, the practically important case of the film imper-

fection in the mode of the decreasing height has been considered under the non-uniform temperature distribution (Fig.11). Again the stability or instability of the crack propagation depends on the temperature gradient like in the case considered in Figs.7a and 8a. The mode of crack nucleation, however, may be affected by the imperfect height as shown in Fig.11a. In this case the crack does not nucleate at the very edge. Instead a blister is born close to the film free edge and then it propagates in both directions.

### 3.3 Convergence of the finite element method

The simulations described in the previous subsection we carried out for the 30 finite element model of the film. The relatively coarse finite element mesh was used because of the numerical problems inherent in the delamination simulation. These problems are the extremely sharp limit points and the closeness of the different parts of the equilibrium path as shown in Figs. 5 and 6. As a result of that the numerical advance along the equilibrium path is exceptionally time-consuming.

In order to estimate the inaccuracy introduced by the coarse mesh we considered the convergence of the results for the increasing number of elements in the case of the film subjected to the uniform thermal load. The critical thermal load equals 585 °C for the 30-element uniform mesh when the dynamic delamination starts. It is equal to 368 °C for the 60-element uniform mesh. The critical temperature values corresponding to the delamination nucleation with of 90 and 120 finite elements are presented in Fig. 12. It is clear from these computations that the more coarse mesh tends to overestimate the critical load as expected by the analogy with a linear finite element analysis. Nonetheless, the specific value of the critical load is not very important for us because only physically approximate model problem is considered. Indeed, this is an idealized one-dimensional delamination of a piece of a real film. The qualitative character of the delamination is more important than the specific numerical magnitudes of thermal loads or displacements.

In order to check the influence of the mesh refinement on the *qualitative* results of the delamination modeling we performed a number of simulations on both coarse (30 elements) and finer (60 elements) meshes. The typical result is shown in Fig.13. Though the qualitative behavior is similar in both cases the finer mesh leads to more flexible structure. Such comparison allows us to accept

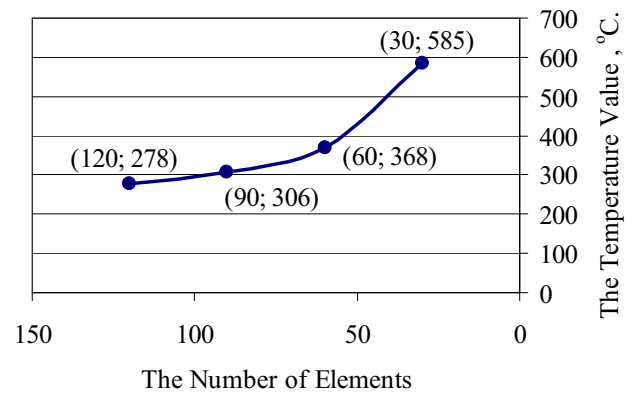


**Figure 12** : The temperature values of the edge crack delamination start in the case of the uniform heating of the film with a different number of elements.

the qualitative results of the simulations on the coarse mesh.

## 4 Conclusions

Qualitative analyses of the thin film delamination (Figs. 7-11) have been carried out on the grounds of the numerical finite element simulations. The computations lead to the following qualitative conclusions regarding delamination behavior of the film for varying thermal loads, bulk and interface material properties:

- Typically, crack nucleates at the free edge of the film.
- The dominant mode of the thermal delamination of the film is shearing (Mode-II-like-crack).
- The gradient of the thermal load can essentially affect the type of the film delamination: it can lead to the stable, i.e. quasi-static, or unstable, i.e. dynamic, propagation of the edge crack.
- The imperfect contact between the film and the substrate can shift the delamination from the edge to the internal area of the film, i.e. a blister is created.
- The imperfect contact between the film and the substrate can lower the critical load of the crack nucleation while transforming the dynamic crack propagation in the quasi-static one.

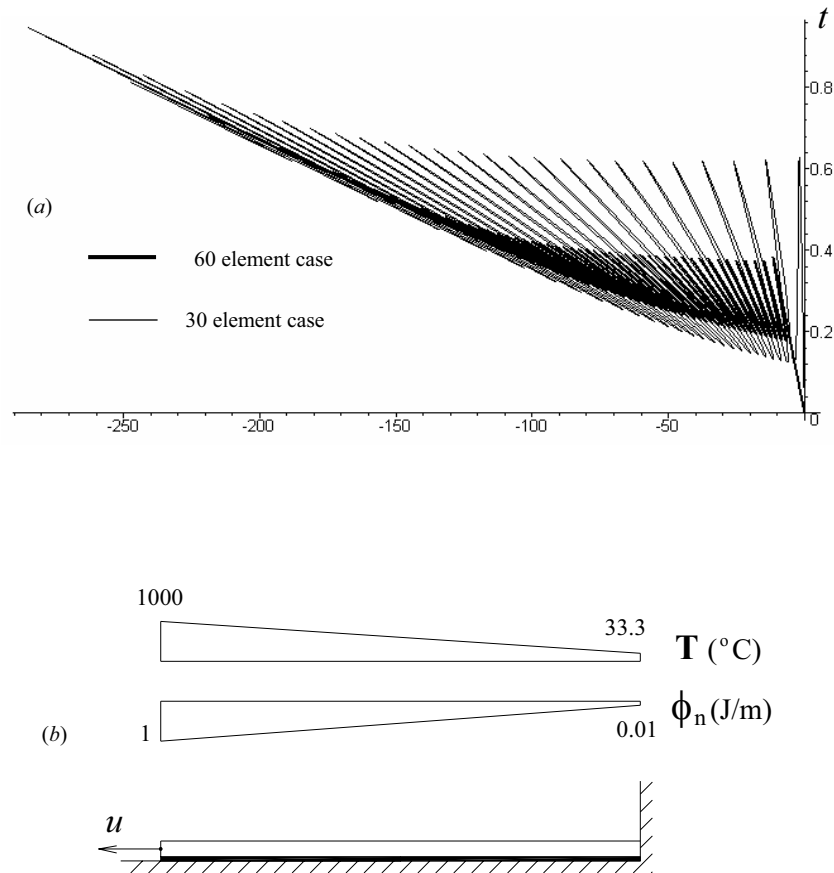


**Figure 13 :** (a) The free end displacements of the thin film with respect to the thermal load factor,  $t$ , for 30 and 60 element cases; (b) The thin film model

- The non-uniform distribution of the thermal expansion coefficient amplifies or reduces the critical thermal load while it has a little effect on the film delamination process as a whole.
- The film thinning at the free edge can lead to the appearance of the unstable blister close to the edge.

Some specific conclusions can be made regarding the arrest of the delamination propagation leading to the stable blister creation:

- The strength of the cohesive surface can significantly affect the blister formation phenomenon.
- The blister nucleation is possible only for some specific combinations of the film and interface properties with suitable thermal load shapes, in all other cases the internal delamination advances dynamically or the edge crack runs.

**Acknowledgement:** This research was supported by the Fund for the Promotion of Research at the Technion.

### References

- Alfano, G.; Crisfield, M. A.** (2001): Finite element interface models for the delamination analysis of laminated composites: mechanical and computational issues. *International Journal for Numerical Methods in Engineering*, 50, 1701-1736.
- Barenblatt, G. I.** (1959): The formation of equilibrium cracks during brittle fracture: General ideas and hypothesis. Axially-symmetric cracks. *Prikl. Matem. I Mekhan (PMM)*, 23, 434-444.
- Bigoni, D.; Ortiz, M.; Needleman, A.** (1997): Effect of interfacial compliance on bifurcation of a layer bounded to a substrate. *International Journal of Solids and Structures*, 34, 4305-4326.

- Camacho, G. T.; Ortiz, M.** (1996): Computational modeling of impact damage in brittle materials. *International Journal of Solids and Structures*, 33, 2899–2938.
- Chandra, N.; Li, H.; Shet, C.; Ghonem, H.** (2002): Some issues in the application of cohesive zone models for metal-ceramic interfaces. *International Journal of Solids and Structures*, 39, 2827-2855.
- Choi, S. R.; Hutchinson, J. W.; Evans, A. G.** (1999): Delamination of multilayer thermal barrier coatings. *Mechanics of Materials*, 31, 431-447.
- Crisfield, M. A.** (1991,1997): *Nonlinear Analysis of Solids and Structures*. Vols 1,2. Wiley, Chichester.
- Dugdale, D. S.** (1960): Yielding of steel sheets containing slits. *Journal of the Mechanics and Physics of Solids*, 8, 100–104.
- Evans, A. G.; Hutchinson, J. W.** (1984): On the mechanics of delamination and spalling in compressed films, *International Journal of Solids and Structures*, 5, 455-466.
- Evans, A. G.; Hutchinson, J. W.** (1995): The thermo-mechanical integrity of thin films and multilayers. *Acta Metal. Mater.*, 43, 2507-2530.
- Frostig, Y.; Sokolinsky, V.** (2000): High-order buckling of debonded (delaminated) sandwich panels with a “soft” core. *AIAA Journal*, 38, 2147-2159.
- Foulk, J. W.; Allen, D. H.; Helms, K. L. E.** (2000): Formulation of a three-dimensional cohesive zone model for application to a finite element algorithm. *Computer Methods in Applied Mechanics and Engineering*, 183, 51-66.
- Geubelle, P. H.; Baylor, J. S.** (1998): Impact-induced delamination of composites: a 2D simulation. *Composites Part B Engineering*, 29B, 589-602.
- Gioia, G.; Ortiz, M.** (1997): Delamination of compressed thin films. *Advances in Applied Mechanics*, 33, 120-193.
- Givoli, D.** (2004): Finite element modeling of thin layers. *CMES: Computer Modeling in Engineering & Sciences*, 5, 497-514
- Hutchinson, J. W.** (2001): Delamination of compressed films on curved substrates. *Journal of the Mechanics and Physics of Solids*, 49, 1847-1864.
- Hutchinson, J. W.; Suo, Z.** (1992): Mixed mode cracking in layered materials. *Advances in Applied Mechanics*, 29, 64-192.
- Kachanov, L. M.** (1976): Separation failure of composite materials. *Polymer Mechanics*, 12, 812-815.
- Kachanov, L. M.** (1988): *Delamination Buckling of Composite Materials*. Kluwer, Dordrecht.
- Keller, H. B.** (1992): *Numerical Methods for Two-Point Boundary-Value Problems*. Dover, NY.
- Kouhia, R.; Mikkola, M.** (1989): Tracing the equilibrium path beyond simple critical points. *International Journal of Numerical Method of Engineering*, 28, 2923-2941.
- Li, W.; Siegmund, T.** (2004): Numerical study of indentation delamination of strongly bonded films by use of a cohesive zone model. *CMES: Computer Modeling in Engineering & Sciences*, 5, 81-90.
- Magnusson, A.; Svensson, I.** (1998): Numerical treatment of complete load-deflection curves. *International Journal of Numerical Method of Engineering*, 28, 2923-2941.
- Mohammed, I.; Liechti, K. M.** (2000): Cohesive zone modeling of crack nucleation at bimaterial corners. *Journal of the Mechanics and Physics of Solids*, 48, 735-764.
- Needleman, A.** (1987): A continuum model for void nucleation by inclusion debonding. *Journal of Applied Mechanics*, 54,525–531.
- Rahulkumar, P.; Jagota, A.; Bennison, S. L.; Saigal, S.** (2000): Cohesive element modeling of viscoelastic fracture: application to peel testing of polymers. *International Journal of Solids and Structures*, 37, 1873-1897.
- Rice, J. R.; Wang, J. S.** (1989): Embrittlement of interfaces by solute segregation. *Material Science and Engineering*, 107, 23–40.
- Riks, E.** (1998): Buckling analysis of elastic structures: a computational approach. *Advances in Applied Mechanics*, 34, 1-76.
- Seydel, R.** (1994): *Practical Bifurcation and Stability Analysis: From Equilibrium to Chaos*. 2<sup>nd</sup> edn, Springer, NY.
- Sheinman, I.; Kardomateas, G. A.; Pelegri, A. A.** (1998): Delamination growth during pre- and post-buckling phases of delaminated composite laminates. *International Journal of Solids and Structures*, 35, 19-31.
- Shield, T. W.; Kim, K. S.** (1992): Beam theory models for thin film segments cohesively bonded to an elastic half space. *International Journal of Solids and Structures*, 29, 1085-1103.

**Shield, T. W.; Kim, K. S., Shield, R. T.** (1994): The buckling of an elastic layer bonded to an elastic substrate in plane strain. *Journal of Applied Mechanics*, 61, 231-235.

**Stroud, W. J.; Krishnamurthy, T.; Smith, S. A.** (2002): Probabilistic and possibilistic analyses of the strength of a bonded joint. *CMES: Computer Modeling in Engineering & Sciences*, 3, 755-772

**Tvergaard, V.; Hutchinson, J. W.** (1992): The relation between crack growth resistance and fracture process parameters in elastic-plastic solids. *Journal of the Mechanics and Physics of Solids*, 40, 1377–1397.

**Volokh, K. Y.; Needleman, A.** (2002): Buckling of sandwich beams with compliant interface. *Computers and Structures*, 80, 1329-1335.

**Wriggers, P.** (1995): Solution strategies for nonlinear equations and of singular points. In: Kounadis AN and Kratzig WB: *Nonlinear Stability of Structures: Theory and Computational Techniques*, Springer, NY.

**Xu, X. P.; Needleman, A.** (1994): Numerical simulation of fast crack growth in brittle solids. *Journal of the Mechanics and Physics of Solids*, 42, 1397–1434.

